



INAOE

An advanced spectrum analysis of optical signals using the non-collinear three phonon light scattering

Technical Report No. 633

Principal contributors:

Alexandre S. Shcherbakov and Adán Omar Arellanes.

National Institute for Astrophysics, Optics, and Electronics
(INAOE), Puebla, Mexico.

National Institute for Astrophysics, Optics, and
Electronics (INAOE),

Puebla, Mexico.

Department for Optics, INAOE

INAOE, 2016

The authors hereby grant to INAOE
permission to reproduce and distribute
copies of this technical report.



Index

1. Introduction	3
2. A three phonon Bragg acousto-optical interaction	5
2.1 General solution for a three-phonon Bragg acousto-optical interaction	5
2.2 Ideal (lossless) local transmission function	6
2.3 Local transmission function with acoustic losses	8
3. Degree of freedom: frequency of 3-phonon acousto-optical interaction	10
4. Photo-elastic effect in TeO₂	13
5. Effect of the acoustic losses: the nonlinear apodization	15
6. Theoretical estimations of the tellurium dioxide-made crystalline acousto-optical cell	17
6.1. Bragg regime of acousto-optical interaction and acoustic beam divergence	17
6.2. Acousto-optical figure of merit for the non-collinear three-phonon AOI in the TeO ₂ -crystal	18
7. Results obtained from proof-of-principal experiments with the TeO₂-made acousto-optical cell	20
7.1. Experiment arrangement	20
7.2. Experimental results	21
8. Conclusions	25
Acknowledgments	26
References	26

ABSTRACT.

The unexpected features of square-law nonlinearity inherent in the non-collinear three-phonon acousto-optical interaction controlled by elastic waves of finite amplitude in birefringent crystals with linear acoustic attenuation are distinguished and investigated. They lead to breakthrough applications of strongly nonlinear three-phonon interaction to linear optical spectrum analysis with ~100% efficiency and qualitatively improved resolution. Principally new physical degree of freedom, unique for this nonlinear phenomenon, is revealed and characterized. The indispensable theoretical developments and proof-of-principle acousto-optical experiments with specially designed wide-aperture tellurium dioxide cell are presented. The obtained experimental results confirm the elaborated approaches promising potentially the highest possible spectral resolution that one can expect in principle from acousto-optical technique within optical spectrum analysis.

Keywords: Nonlinear optics, parametric processes, Nonlinear wave mixing, Acousto-optical devices, Spectroscopy of high resolution.

1 INTRODUCTION

Strongly nonlinear behavior of light beams within Bragg acousto-optical interaction (AOI) in an anisotropic medium with linear acoustic attenuation can be experimentally detected without any observable effect of the AOI process on an elastic wave. We study the case when similar process is governed by the elastic wave of finite amplitude exhibiting the linear attenuation. In this case, the elastic wave amplitude is described by an independent non-homogeneous (due to the linear acoustic losses) wave equation in a given field approximation, while light beams amplitudes are governed by a set of combined differential equations with square law nonlinearity. This acousto-optical (AO) nonlinearity is parametric by its nature; the elastic wave amplitude controls it. Usually, the Bragg AOI incorporates conserving both the energy and the momentum for each partial act of a three-particle interaction. When the central cross-section of two wave vector surfaces, reflecting two eigen-states of light polarization in optically anisotropic media, is crossed by the direct line, placed close enough to a joint center of those surfaces and being collinear to the wave vector of an elastic wave, one can obtain up to four points of intersection [1]. This fact indicates that the chosen geometry of AOI in anisotropic medium allows, as a maximum, the four-orders of light deflected by an elastic wave in the Bragg regime. In the particular case, when these four intersections are equidistant, a four-order AOI can be provided by only one harmonic elastic (i.e. acoustic) wave, as it is shown for a uniaxial tellurium dioxide crystal in Fig. 1a. By this is meant that, under certain conditions, i.e. at the exactly chosen angle of light incidence on the selected crystal cut and at fixed frequency of the acoustic wave, it will be possible to realize the Bragg AOI caused by sequential participation of the first, second, and third phonons. As a result, a three-phonon AOI will be observed.

Historically, this phenomenon had been revealed in 80s past century [2] and then studied additionally [3,4]. Time to time some non-systematic theoretical attempts had been undertaken in a view of considering potential applications of this phenomenon to performing various logic-based operations all-optically [5]. Such a place of three-phonon AOI can be easily explained first of all due to its strongly nonlinear nature and the nonlinear behavior of light beams within this regime of interaction. Together with this, the three-phonon AOI was traditionally mentioned together with the two-phonon anomalous AOI for crystallographic orientation in the vicinity of an optical axis in the tellurium dioxide crystal. However, availability of the corresponding vector diagram does not guarantee the effective process of such an AOI in a material. Recently [1], it has been demonstrated

that within that geometry the three-phonon AOI has very low efficiency in tellurium dioxide due to almost zero efficiency inherent in the middle step of AOI, which is normal in its physical nature.

The prime objectives of our studies are to reveal physically new features inherent in the nonlinearity of three-phonon AOI controlled by elastic waves of finite amplitude. We clarify the details of this nonlinearity both theoretically and experimentally in wide-aperture crystals with moderate linear acoustic attenuation and analyze the principle opportunity of applying this phenomenon to the optical spectrum analysis with the considerably (about three times) qualitatively advanced spectral resolution. Identifying a sequence of the local unit-level maxima in the distribution of light scattered into the third order, which occur as the acoustic power density grows, gives a chance to optimize the transmission function profile specific to each maximum. Fortunately, already the first maximum has really desirable profile of transmission function at the fixed angle of incidence for the incoming light beam with a wide optical spectrum.

Then, we deduce that non-collinear three-phonon AOI can have ~100% efficiency due to an additional birefringence factor, distinguished within this nonlinear phenomenon. It can be achieved at the fixed optical wavelength for a wide spectrum of acoustic frequencies or at the fixed acoustic frequency for a wide range of optical wavelengths. However, only the second option provides linearity between the input and output signals, i.e. linear dependence of the scattered light intensity on the incident one, within strongly nonlinear three-phonon AOI, which is able additionally to treble the spectral resolution, see Fig. 1b. This is why we choose the second option with the fixed acoustic frequency promising a breakthrough approach to AO technique of the pattern optical spectrum analysis with greatly progressed spectral resolution. Thus one has to note that similar approach demonstrates a pioneer possibility to apply the non-collinear three-phonon AOI to practical usage for the first time to our knowledge. Such a possibility is demonstrated at first theoretically for the tellurium dioxide (TeO_2) crystal of tetragonal symmetry as an example. Then, it is confirmed during the proof-of-principle experiments with a specially designed unique wide-aperture acousto-optical cell (AOC), based on the tellurium dioxide crystal and governed by acoustic waves of finite amplitude with linear acoustic attenuation.

2. A THREE-PHONON BRAGG ACOUSTO-OPTICAL INTERACTION

2.1. General solution for a three-phonon Bragg AOI

Let us start from the cross-sections of surfaces for the wave vectors describing the three-phonon AOI in crystals, see Fig. 1. Strongly nonlinear behavior of optical components with the Bragg AOI in anisotropic medium can be achieved in usual experiment without any observable influence of the scattering process on the acoustic wave. In this case the amplitude of acoustic wave is governed by a wave equation that includes the linear acoustic attenuation. Usually, the Bragg AOI incorporates conserving both the energy and the momentum for each partial act of a one-phonon light scattering [6], but one has to take into account both angular and frequency mismatches in the wave vectors of interacting waves. Under certain conditions, i.e. at well-determined angle θ_0 of light incidence on selected crystal cuts and at specifically chosen fixed frequency of acoustic wave, one can observe Bragg scattering of the light caused by participating three phonons and the conservation laws are given by $\nu_1 = \nu_0 + f_3$, $\vec{k}_1 = \vec{k}_0 + \vec{K}$, $\nu_2 = \nu_0 + 2f_3$, $\vec{k}_2 = \vec{k}_0 + 2\vec{K}$, $\nu_3 = \nu_0 + 3f_3$, and $\vec{k}_3 = \vec{k}_0 + 3\vec{K}$ simultaneously (ν_m , \vec{k}_m and f , \vec{K} are the frequencies and wave vectors of light and acoustic waves, $m = 0, 1, 2, 3$) [2]. Such a five-wave process occurs at the frequency f_3 of acoustic wave, peculiar to the three-phonon AOI, which can be geometrically found directly from Fig. 1a, as

$$f_3 = \lambda^{-1} V b_3, \quad (1)$$

where $b_3 = (0.5 |n_E^2 - n_O^2|)^{1/2}$ is the dispersive birefringence factor and $n_E \neq n_O$ are the current (and still not quite well determined) refractive indices of a crystal, V is the ultrasound velocity, λ is the incident light wavelength. The polarization states of light in various orders of scattering can be orthogonal to each other, whereas the frequencies of light beams in the first, second, and third orders are shifted by f_3 , $2f_3$ and $3f_3$ relative to the zero order light beam. The optimal angle for light incidence θ is given by $\sin \theta = 3(2 |n_E^2 - n_O^2|)^{1/2} / (4n_O)$.

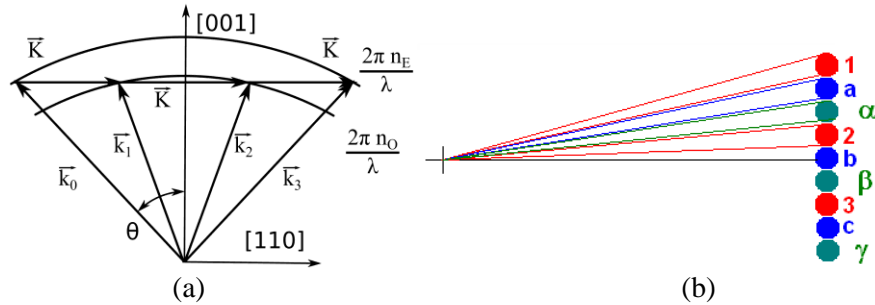


Fig. 1. The non-collinear three-phonon AOI vector diagram (a) and scheme of tripling the spectral resolution (b). Spots 1, 2, 3,... are related to a one-phonon AOI, the additional spots a, b, c,... describe a two-phonon AOI, while the extra-spots α , β , γ ,... correspond to the three-phonon AOI refining the spectral resolution.

Originally equations for the complex amplitudes $C_m(x)$ of light waves ($m = 0, 1, 2, 3$), appearing due to a quasi-stationary three-phonon Bragg light scattering by an acoustic wave of the amplitude U , are given by [2]

$$a) \frac{dC_0}{dx} = -q_a U C_1 \exp(-i\eta_0 x),$$

$$\begin{aligned}
\text{b) } \frac{dC_1}{dx} &= q_a U C_0 \exp(i\eta_0 x) - q_n U C_2 \exp(-i\eta_1 x), \\
\text{c) } \frac{dC_2}{dx} &= q_n U C_1 \exp(i\eta_1 x) - q_a U C_3 \exp(-i\eta_2 x), \\
\text{d) } \frac{dC_3}{dx} &= q_a U C_2 \exp(i\eta_2 x).
\end{aligned} \tag{2}$$

The coordinate x is directed orthogonally to the acoustic beam propagation, i.e. almost along the direction of all the light beams passing. Products of the factors $q_{n, a}$ of AOI for normal and anomalous light scattering, respectively, and the acoustic wave complex amplitude U can be expressed as $\sigma_{n, a} = q_{n, a} U = \pi (M_2^{(n,a)} P/2)^{1/2} / (\lambda \cos \theta)$. The constant angular-frequency mismatches $\eta_m = k_{m, x} - k_{m+1, x}$ are explained in terms of x -components for light wave vectors. However, in the case related to acoustic wave of finite amplitude in a medium with the linear acoustic losses, Eq.(2) has to be complemented by a wave equation for the complex amplitude $U(z,t)$ of a slow acoustic wave

$$\frac{\partial U}{\partial z} + \frac{1}{v} \frac{\partial U}{\partial t} = -\alpha U, \tag{3}$$

passing exactly along the axis z associated with optical aperture of an AOC. Here, the axis z is orthogonal to the axis x , v is the velocity of that acoustic wave, and the factor α describes the linear acoustic attenuation. The simplest boundary conditions $|C_0(x=0)|^2 = I$, $C_{1,2,3}(x=0) = 0$ and exploit the conservation law $|C_0|^2 + |C_1|^2 + |C_2|^2 + |C_3|^2 = I$, resulting from Eq.(2), where I is the intensity of continuous-wave incident light beam. Then, one can use the relations $\eta_0 \equiv \eta$, $\eta_1 = 3\eta$, and $\eta_2 = 7\eta$ [2] to obtain the evolution equation for the complex amplitude $C_3(x)$ of the light scattered into the third order

$$\begin{aligned}
&\frac{d^4 C_3}{dx^4} - 28i\eta \frac{d^3 C_3}{dx^3} + [\sigma_n^2 + 2\sigma_a^2 - 239\eta^2] \frac{d^2 C_3}{dx^2} + \\
&i\eta[644\eta^2 - 11\sigma_n^2 - 28\sigma_a^2] \frac{dC_3}{dx} + \sigma_a^2 [\sigma_a^2 - 110\eta^2] C_3 = 0.
\end{aligned} \tag{4}$$

with the boundary conditions $C_3(x=0) = (dC_3/dx)(x=0) = (d^2C_3/dx^2)(x=0) = 0$ and $(d^3C_3/dx^3)(x=0) = \sigma_n \sigma_a^2$. It is seen that the ratio $\chi = \sigma_n/\sigma_a$ reflects the properties of an AO-material in the chosen direction of acoustic wave propagation and plays very important role here.

2.2. Ideal (lossless) local transmission function

First, we analyze Eqs. (2) and (3) with an ideal lossless case, when $\alpha = 0$ and the acoustic wave has a constant amplitude $U \equiv U_0$ along the optical aperture of an AOC. At the absence of any mismatch $\eta = 0$, one yields

$$C_3(x) = \frac{\sqrt{2}}{\sqrt{4+\chi^2}} \left\{ \frac{\sin \left[\frac{\sigma_a x}{\sqrt{2}} \sqrt{2+\chi^2 - \chi \sqrt{4+\chi^2}} \right]}{\sqrt{2+\chi^2 - \chi \sqrt{4+\chi^2}}} - \frac{\sin \left[\frac{\sigma_a x}{\sqrt{2}} \sqrt{2+\chi^2 + \chi \sqrt{4+\chi^2}} \right]}{\sqrt{2+\chi^2 + \chi \sqrt{4+\chi^2}}} \right\}. \tag{5}$$

At $\eta \neq 0$, one can calculate the following 3D- and 2D-plots with $q_a = 1.00$ and $q_n = 1.15$. It is seen that the ratio $\chi = \sigma_n/\sigma_a$ reflects the properties of an AO-material in the chosen direction of acoustic wave propagation and plays very important role here. Figure 2a exhibits a sequence of the unit level maxima, whose widths of profiles are increasing as the dimensionless coordinate $\sigma_a x$ grows.

A pair of 2D-plots with $\eta = 0$ in Fig. 2b shows that when $\chi = 1.15$ (solid line) one can see a sequence of the unit level maxima, but when, for example $\chi = 1.0$ (dashed line), this sequence becomes destroyed rather fast as the parameter χ is varied. Nevertheless, the first maxima for both these cases are very close to one another.

Initially, let us concentrate our attention on the dynamics (behavior) of the first maximum, which is the narrowest in Fig. 2a, but it can be achieved simpler than the others due to relatively low level of the acoustic power density required for its achievement. Whereas one of the important factors, affecting the magnitude of this maximum and determining the needed acoustic power, is the ratio χ . Figure 3 represents a set of 2D-plots reflecting the dependences of light intensity, scattered into the first maxima inherent in the three-phonon AOI, with various ratios χ lying between 0.5 and 2.0. The analogous 3D-plot is depicted in Fig. 3c.

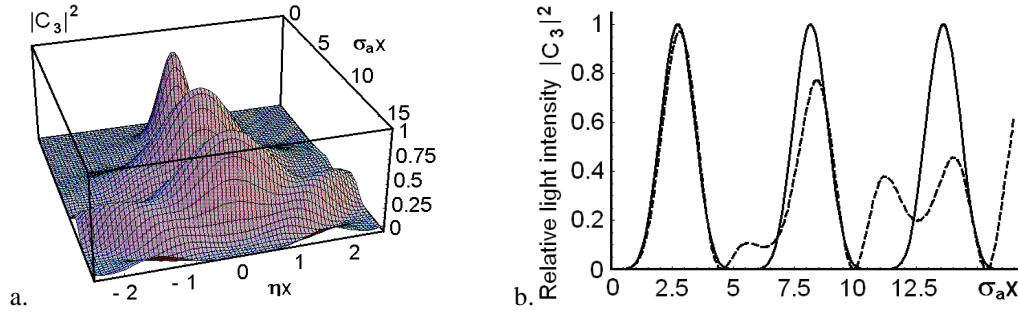


Fig. 2. Relative light intensity $|C_3|^2$ distributions: (a) 3D-plot in the coordinates $\sigma_a x$ and ηx ; (b) a pair of 2D-plots with $\eta = 0$; when $\chi = 1.15$ (solid line) one can see a sequence of the unit level maxima, but when, for example $\chi = 1.0$ (dashed line), this sequence becomes destroyed.

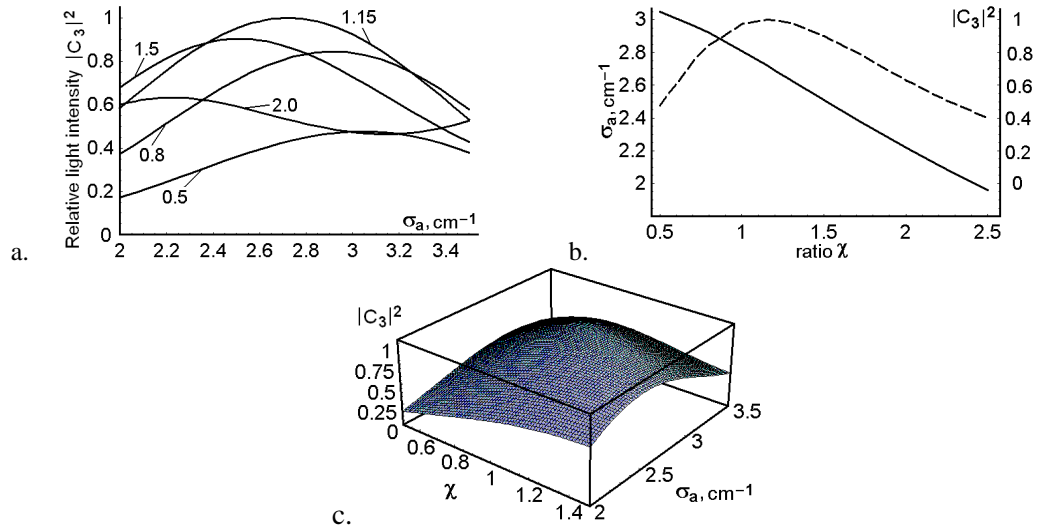


Fig. 3. Relative light intensity $|C_3|^2$, scattered into the first maxima inherent in the three-phonon AOI, with various ratios χ lying between 0.5 and 2.0 due to the acoustic power density described by σ_a with $\eta = 0$: a) $|C_3|^2$ vs. the parameter σ_a , b) $|C_3|^2$ vs. the ratio χ , the inter- relation between σ_a and χ is shown too, and c) The corresponding 3D-plot with various ratios χ lying between 0.5 and 1.5 due to the acoustic power density described by σ_a with $\eta = 0$.

These 2D-plots predict that choosing the exact value $\chi = 1.15$ is maybe not too critical for experimental verification of our analysis. This is rather important deduction because the ratio χ is usually the property of a material, which can be varied not easily. The plots in Fig. 4 show a triplet of the first transmission functions inherent in the non-collinear three-phonon light scattering.

It is seen that the first maximum exhibits the narrowest transmission function, but it can be observed at the lowest value of the dimensionless coordinate $\sigma_a x = 2.72$, which is the most attractive for applications associated with low-power signals. Figure 4 depicts the first transmission function of the width for $\sigma_a x = 2.72$ in detail; the whole width is equal to $\eta_\Sigma x = |\eta_-| x + \eta_+ x \approx 0.76$ at the 0.405-level. As before, we are using the level of 0.405 taken from the Rayleigh criterion [7] due to operating over sinc^2 signals. This level coincides also with the -4 dB level exploited as well.

Because of the mismatch had been originally [2] defined as $\eta = \pi \lambda f_3 (\Delta f)/(n_0 V^2)$, one can find that the frequency bandwidth of a three-phonon AOI at the 0.405-level is determined by

$$\Delta f \approx 0.76 n_0 V^2 / (\pi \lambda f_3 L). \quad (6)$$

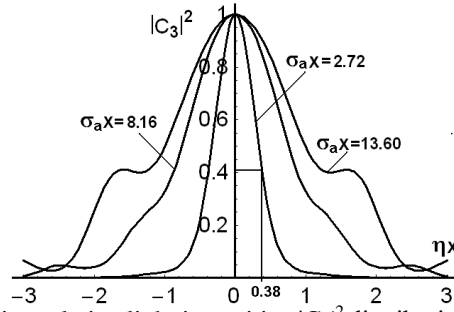


Fig. 4. Transmission functions i.e. relative light intensities $|C_3|^2$ distributions with $\eta \neq 0$ and $\chi = 1.15$ at the isolated points $\sigma_a x = 2.72, 8.16, \text{ and } 13.60$ specific to the unit-level maxima from Fig. 2b.

2.3. Local transmission function with acoustic losses

In reality $\alpha \neq 0$, and Eq.(1c) has the general solution $U(z) = U_0 \exp(-\alpha z)$ in the tracking coordinates, while U_0 is now the initial magnitude of that acoustic wave. By this it means that the above-noted solution has to involve a dependence on the coordinate z as $\sigma_a = q_a U_0 \exp(-\alpha z)$ and to take the form $C_3(x, z)$. As a result, one arrives at the modified 3D-distribution similar to Fig. 2a and plots similar to Fig. 2b with $\eta x = 0$.

Now, one can consider additionally the dimensionless attenuation parameter $a = \alpha z$ describing the linear acoustic losses in a material. With separating the parameter, which includes two dimensionless coordinates $\sigma_a x$ and ηx , characterizing the acoustic power density and the frequency mismatch, as well as the above-included one $a = \alpha z$. Thus one can obtain the following 2D-distributions that should be interpreted using 3D-distribution in Fig. 1 for the cases of $a = 0$. These distributions show that growing the parameter $a = \alpha z \in [0, 0.3, 0.5]$ leads in fact only to scaling these distributions along the horizontal axis $\sigma_a x$ when $\eta x = 0$, see Fig. 5.

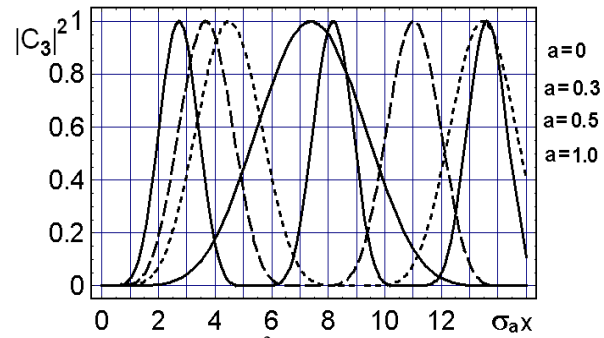


Fig. 5. The 2D-plots for relative light intensity $|C_3|^2$ distributions vs. in the dimensionless coordinate $\sigma_a x$ with $\eta = 0$ and $q_n/q_a = 1.15$; solid lines are for $a = 0$ and 1.0 , dashed line is for $a = 0.3$, and dotted line is for $a = 0.5$. One can see a sequence of the unit level maxima and the dynamics of scaling due to effect of linear acoustic losses.

3. DEGREE OF FREEDOM: FREQUENCY OF 3-PHONON ACOUSTO-OPTICAL INTERACTION

Now, we make a breaking-through step in theory of the non-collinear three-phonon AOI, see Fig. 6. This step can be represented in terms of two surfaces for the refractive indices of ordinary (see an internal dark sphere) and extraordinary (see an external bright ellipsoid) light waves ($N_E \geq N_O$) for a tetragonal crystal at the fixed optical wavelength λ . The parameters of both these surfaces can be varied depending on λ due to the expected dispersion of a crystal within the visible range. The vertical axis in Fig. 6 is oriented along the optical axis [001], while two horizontal axes can be oriented depending on the chosen material and the excited elastic mode. Then, this figure includes a multi-vector diagram illustrating the three-phonon AOI through the tilt angle, which use the same acoustic frequencies and birefringence factor b . The quartets of vectors, going from the geometric center of surfaces, represent the optical wave vectors describing the corresponding orders of AOI, whereas sequentially co-directed trio of the acoustic wave vectors represent three-phonon processes. This vector diagram reflects existence of the revealed here additional physical degree of freedom inherent in the nonlinearity of three-phonon AOI. In consequence of this degree of freedom one can exploit the fixed frequency f_3 to exert control over various optical wavelengths scattered through different angles. In this case, one has to consider two pairs of surfaces peculiar to the refractive indices of ordinary and extraordinary light waves for a tetragonal crystal and each similar pair of surfaces will correspond to an individual light wavelength λ . Nevertheless, each vector diagram for two different nonlinear processes of three-phonon AOI will include acoustic vectors \vec{K} of the same lengths characterizing the same acoustic frequency f_3 . To perform a three-phonon AOI at a given acoustic frequency one has to consider involving a tilt angle into geometry of similar AO process. In so doing, one has to select the concrete optical wavelength for an analysis. Tellurium dioxide is a uniaxial crystal, so that $n_O \equiv N_O$ is the main refractive index for the ordinary state of polarization, while n_E depends on a direction in a crystal and has the form of an ellipsoid, see Fig. 6. We are interested in tilts from the [001]-axis, therefore, one can consider the angle $\phi \in [0, \pi/2]$ of a tilt from the [001] axis, see Fig. 6.

Let us estimate the acoustic frequency required for three phonon AOI in a crystal, which can exhibit optical activity. For this matter we took the index surface equations for a positive uniaxial crystal in the form [4] of

$$\frac{n_{O,E}^2(\vartheta) \cos^2 \vartheta}{N_O^2 (1 \mp \delta)^2} + \frac{n_{O,E}^2(\vartheta) \sin^2 \vartheta}{N_{O,E}^2} = 1, \quad (7)$$

where $N_{O,E}$ and $n_{O,E}$ are the main and current ordinary and extraordinary refractive indices of a birefringent crystal, respectively; ϑ is the angle between the optical axis and the incident light beam. Then, one has the optical activity factor $\delta = 0.5 |1 - n_E(\vartheta = 0)/n_O(\vartheta = 0)|$ which characterizes the contribution from optical activity, so that $\delta = 0$ in the absence of optical activity. To simplify the calculations and visualization of the wave vectors diagram one can introduce the tilt angle ϕ between the optical axis and the plane of light scattering, see Fig. 6. Here, axes X and Y are taken depending on the real axes in a crystal.

In the Cartesian coordinates, the equations for the index surfaces take the form

$$\frac{x^2}{N_{O,E}^2} + \frac{z^2}{N_O^2 (1 \mp \delta)^2} + \frac{y^2}{N_{O,E}^2} = 1 \quad (8)$$

for ordinary and extraordinary refractive indices, respectively. We resolve a set of Eqs.(8) relative to the variable y , because a trio of the acoustic wave vectors is lying in a sequence along this axis.

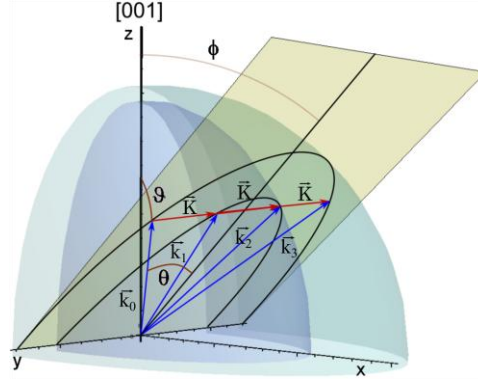


Fig. 6. Index surfaces for the ordinary refractive index (inner ellipsoid) and the extraordinary refractive index (outer ellipsoid). The two semi-ellipses represent the intersections of these ellipsoids with the plane of light scattering (yellow plane); declined by the tilt angle ϕ .

In so doing, one estimates the position, for which the distance of intersection with the internal surface will be the same as the distance between internal and external surfaces. In terms of the wave vector diagram (see Fig. 6), this condition is the requirement for the three-phonon light scattering to exist. This condition would be satisfied for several tilt angles and will give us the acoustic frequency required for three phonon AOI in a crystal. As a result, one yields a new formula for the acoustic frequency f_3 required for the three phonon AOI in a crystal, which can exhibit optical activity.

$$f_3 = \frac{2V}{\lambda(1-\delta)} \sqrt{\frac{N_O^2(\delta-1)^2 [4N_E^2\delta + (N_E^2 - N_O^2)(\delta^2-1)^2 \cdot \tan^2\phi]}{9N_O^2(1+\delta)^2 - N_E^2(\delta-1)^2 + 8N_O^2(\delta^2-1)^2 \cdot \tan^2\phi}}. \quad (9)$$

One can see from Eq.(9) that this frequency strongly depends on two parameters: the tilt angle ϕ and has the optical activity factor δ .

To make our consideration more concrete an appropriate AO crystalline material has to be selected for the further analysis. Within similar selection of a material, one has to say that there are not too many possibilities of exploiting either longitudinal or shear elastic modes, passing along various crystallographic directions. The analysis has shown that in fact only one material, namely, tellurium dioxide (TeO_2) single crystal, exhibiting the optical activity had been previously analyzed theoretically due to its crystal-physical properties and considered practically for performing any experiments oriented on a three-phonon AOI. In part, such a selection was historically motivated by very high efficiency of light scattering and not too high acoustic frequency needed for excitation of a three-phonon AOI in this material. This crystal belongs to the 422 – tetragonal symmetry group. It has spectral transmission band $\Delta\lambda = 0.35 - 5.0 \mu\text{m}$ and a pair of dispersive refractive indices, whose main values are $N_O = 2.3297$ and $N_E = 2.4956$ at the wavelength $\lambda = 488 \text{ nm}$ [8]; its material density is equal to $\rho \approx 6.0 \text{ g/cm}^3$ [9]. This crystal is potentially suitable for effective non-collinear three-phonon AOI and allows pure slow-shear elastic mode with the wave vector $\vec{k} \parallel [110]$, the displacement vector $\vec{u} \parallel [1\bar{1}0]$, the phase velocity $V_s \approx 0.616 \cdot 10^5 \text{ cm/s}$, and the acoustic wave attenuation factor $\Gamma \approx 290 \text{ dB/(cm GHz}^2)$, which gives the amplitude factor α of losses in the form of $\alpha (\text{cm}^{-1}) = 0.1152 \Gamma f^2$.

With $\delta \sim 10^{-4}$, Eq. (9) is plotted in Fig. 7 to appreciate the relations between the tilt angle ϕ and the acoustic wave frequency f_3 and the experimental data related to the ellipticity of the incident light beam in the particular case of the TeO_2 crystal working at $\lambda = 488 \text{ nm}$.

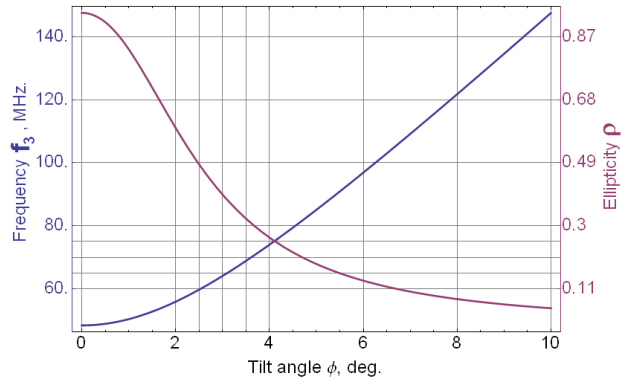


Fig. 7. Acoustic frequency and ellipticity of the incident light vs. the tilt angle ϕ needed for the three-phonon AOI in the TeO_2 crystal.

These parameters can be exploited to chose a balance between decreasing the central acoustic frequency (to minimize the effect of acoustic losses) and reducing the ellipticity of light beams (to simplify conditions for potential experiments with TeO_2 crystal made AOC). One should take into account that reliable realization of a given value for the ellipticity in an AOI-area is not so easy during the experiment.

4. PHOTO-ELASTIC EFFECT IN TeO₂

Generally, when the elastic wave is passing through a medium, the dielectric impermeability tensor $\hat{\kappa}$ becomes to be perturbed under action of mechanical deformations γ and takes the form $\hat{\kappa} + \zeta$, where the symmetrical tensor $\zeta = p \hat{\gamma}$ of the 2-nd rank represents small addition to the tensor $\hat{\kappa}$, while p is the tensor of the 4-th rank of photo-elastic coefficients and $\hat{\gamma}$ is the deformation tensor [10]. When the slow-shear acoustic mode is passing along the $[1\bar{1}0]$ -axis of a TeO₂-crystal and its displacement vector is oriented along the $[110]$ -axis, one can find $\zeta = p \hat{\gamma} = 0.5 (p_{11} - p_{12}) (\bar{x}_1 \cdot \bar{x}_1 - \bar{x}_2 \cdot \bar{x}_2)$ in the dyadic form. Then, it is well known that physical axes of the optical indicatrix determine a pair of eigen-vectors of the electric induction in a crystal. That is why the quadratic form $p_{eff} = \bar{d}^{(S)} \zeta \bar{d}^{(i)}$ describes the effective photo-elastic constant p_{eff} of AOI, i.e. the efficiency of converting the incident state of light polarization, described by the unit vector $\bar{d}^{(i)}$ oriented along the incident electric induction $\bar{D}^{(i)}$ into the scattered state of light polarization, characterized by the unit vector $\bar{d}^{(S)}$ oriented along the scattered electric induction $\bar{D}^{(S)}$. Now, one may exploit a reduced version of the addition matrix $\tilde{\zeta}$ instead of ζ , which is normalized by the factor $0.5 (p_{11} - p_{12})$ as well as \tilde{p}_{eff} normalized in the same way. Then, only the ellipticity ρ can reflect the angular declination from the optical axis for the light beams, because all the angles of incidence and scattering lie in a range of a few degrees. The reduced matrix of small additions represents a minor of the matrix ζ in the form $\tilde{\zeta} = \bar{x}_1 \cdot \bar{x}_1 - \bar{x}_2 \cdot \bar{x}_2 + iG_{33} (\bar{x}_1 \cdot \bar{x}_2 - \bar{x}_2 \cdot \bar{x}_1)$, which includes the optical activity. The value of G_{33} can be found experimentally for a TeO₂, so that [1] $G_{33} \approx 4.26 \times 10^{-5}$ at $\lambda = 488$ nm. Thus with conserving the polarization state ($i \rightarrow i$), i.e. within the normal AOI, as well as with changing the polarization state ($i \rightarrow j$), i.e. with the anomalous AOI, (here, $i, j = 1, 2; i \neq j$) one can find

$$\begin{aligned}
 \text{a) } |\tilde{p}_{eff}(i \rightarrow i)| = p_n &\approx \frac{1 - \rho^2 - 2\rho G_{33}}{1 + \rho^2}, \\
 \text{b) } |\tilde{p}_{eff}(i \rightarrow j)| = p_a &\approx \frac{2\rho + (1 - \rho^2)G_{33}}{1 + \rho^2}, \\
 \text{c) } \frac{q_n}{q_a} &\approx \frac{1 - \rho^2 - 2\rho G_{33}}{2\rho + (1 - \rho^2)G_{33}}. \tag{10}
 \end{aligned}$$

The plots of the corresponding numerical estimations for these formulas vs. the ellipticity ρ are presented in Fig. 8.

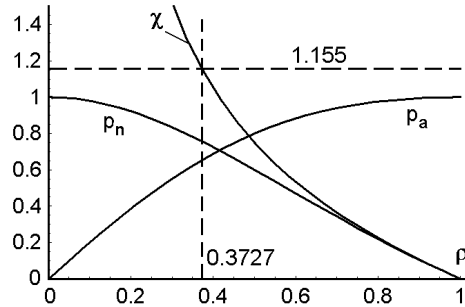


Fig. 8. Relations between the photo-elastic constants p_a and p_n .

One can find that the efficiency of normal light scattering ($p_n \approx 0.756$) exceeds the efficiency of anomalous one ($p_a \approx 0.655$) in a TeO_2 -crystal at the chosen orientation with $\chi = |p_n / p_a| \approx 1.155$. Namely, one has found the ellipticity $\rho \approx 0.37275$, which requires the declination angle $\vartheta \approx \phi \approx 3.142^\circ$ and the central acoustic frequency $f_3 \approx 65$ MHz.

5. EFFECT OF THE ACOUSTIC LOSSES: THE NONLINEAR APODIZATION

At this point we will not motivate in detail our selection of the level B for linear acoustic losses per optical aperture D of the tellurium-dioxide-made AOC. Nevertheless, together with traditionally exploited value $B = 4$ dB [7], the values $B = 2.45 - 7.35$ dB will be taken as well in a view of principle possibility to correct them later by the needed apodization. Choosing these values allows us to avoid unnecessarily strong limitations for this stage of studies. More detailed analysis can be started proceeding from the optical aperture $D = 6.2$ cm of the AOC, restricted by an available sample of the chosen crystalline material. In an attempt of avoiding the effect of optical activity, one has to take the tilt angle 3.0° as a minimum and estimate the ellipticity by about of $\rho \approx 0.3727$ [4]. This choice gives the central acoustic frequency $f_3 \approx 65.0$ MHz at $\lambda = 488$ nm, the acoustic losses $\gamma \approx 1.225$ dB/cm and $\alpha \approx 0.1411$ cm⁻¹.

Taking the above-chosen central frequency f_3 , one can find the following levels of acoustic losses $B_k = D_k \Gamma f_3^2$ per the corresponding aperture D_k at this fixed frequency f_3 . Here, the index $k = \{2 - 6\}$ reflects the optical aperture of a crystal in centimeters. This approach differs from an algorithm of the analysis developed recently [11], because now exactly the central acoustic frequency f_3 and light wavelength λ are fixed, while the optical aperture is varied.

Since the phase velocity $V_s \approx 0.616 \cdot 10^5$ cm/s is already known, one can theoretically estimate the expected frequency $\delta f_{k,T} = V(3D_k)$ and spectrum $\delta \lambda_{k,T} = \lambda^2 / (3b D_k)$ resolutions (here, $b = f_3 \lambda / V$) for each aperture D_k , see Table 1.

For this set of the optical apertures D_k , the first unit level maxima can be reached at a set of the optimized values $(\sigma_a x)^{(k)}_{1,Opt}$ in such a way that both the falling down wings of the corresponding light intensity distributions $|C_3|^2$ have the levels $|C_3|^2_{min,K}$.

Table 1. Theoretical characterization of TeO₂ AOC.

D_k , cm	B_k , dB	$\delta f_{k,T}$, kHz	$\delta \lambda_{k,T}$, Å	$(\sigma_a x)^{(k)}_{1,Opt}$	$ C_3 ^2_{min,K}$	β_k	κ_k
2	2.45	10.27	0.771	3.105	0.86	0.302	1.0113
3	3.68	6.85	0.514	3.29	0.72	0.675	1.02443
4	4.9	5.13	0.385	3.47	0.56	1.16	1.04345
5	6.13	4.11	0.309	3.64	0.405	1.808	1.06867
6	7.35	3.42	0.257	3.82	0.28	2.546	1.0984

After performing the above-proposed optimization, one can use the found values of $(\sigma_a x)^{(k)}_{1,Opt}$, which provide more symmetric distributions presented in Fig. 9. An example of the corresponding 3D-distribution with the $D_4 = 4.0$ cm and $(\sigma_a x)^{(4)}_{1,Opt} \approx 3.47$ is presented in Fig. 10. Looking at these plots, one can find that the combined influence provided by acousto-optical nonlinearity and linear acoustic losses leads to the some equivalent apodization of initially flat incident light beam, see solid lines in Fig. 9.

To describe the Gaussian apodization for a flat incoming light beam with the field amplitude A_0 we use the approach based on the apodization parameter β and described previously [11].

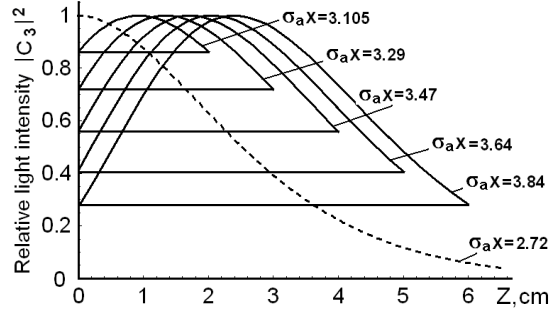


Fig. 9. Optimized 2D-profiles of the light distributions at the output facet of the tellurium dioxide-made AOC at $f_3 = 65.0$ MHz with $\alpha \approx 0.1411$ cm $^{-1}$ for the corresponding D_k (solid lines); the dashed line is for a non-optimized profile.

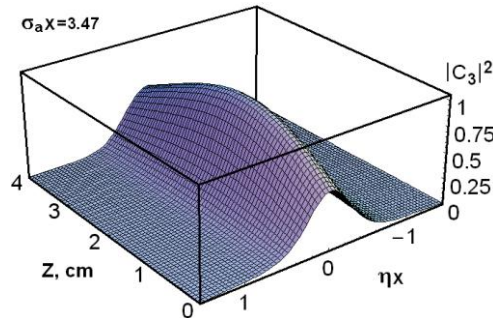


Fig. 10. An example of an optimized 3D-profile of the issuing light distribution at $f_3 = 65.0$ MHz and $(\sigma_a x)_{1,Opt}^{(4)} \approx 3.47$ with $D_4 = 4.0$ cm, and $\alpha \approx 0.1411$ cm $^{-1}$.

In the case of the apodization parameter $\beta \approx 0$, an ideal normalized profile of a resolvable spot has full width equal to unity in terms of the dimensionless coordinate $u = w D/\lambda F$ at the intensity level 0.405 in the focal plane of the integrating lens with the focal distance F . The required corrections to theoretical width of a resolvable spot, destroyed by the linear acoustic losses when $\beta \neq 0$, can be made using the correction factors κ . The needed values of these factors are: $\kappa_k \approx 1.01139, 1.02443, 1.04345, 1.06867, \text{ and } 1.09884$, i.e. the main lobe has broadening by about 1.14, 2.44, 4.35, 6.87, and 9.88 % due to the effect of linear acoustic losses for each β_k , respectively. Thus, the performed apodizations, provided by properties of an AOC near the first maximum, are not deep enough (they equal to -14 to -18 dB for the first side lobe) to improve significantly the dynamic range of potential optical spectrum analysis, see Fig. 11.

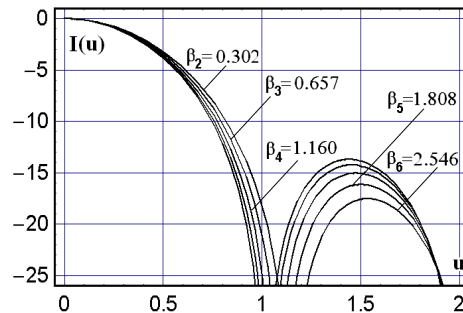


Fig. 11. Theoretical logarithmic profiles of resolvable spots with the dimensionless apodization parameters β_k .

6. THEORETICAL ESTIMATIONS OF THE TELLURIUM DIOXIDE-MADE CRYSTALLINE ACOUSTO-OPTICAL CELL

6.1 Bragg regime of acousto-optical interaction and acoustic beam divergence

The length L and central frequency f_3 of Bragg AOI in a crystal are restricted by well-known inequality for the Klein-Cook parameter $Q = 2 \pi \lambda L f^2 / (n_0 V^2) \gg 1$ [12]. For the slow-shear acoustic mode passing along the $[1\bar{1}0]$ -axis in tellurium dioxide, one has $V = 0.616 \times 10^5$ cm/s and $n_0 \equiv N_O \approx 2.3297$ at $\lambda = 488$ nm. With the above-chosen $f_3 = 65$ MHz, one can find $L_{\min} \gg 0.00685$ Q cm. Taking the limiting value $Q = 4 \pi$, as it had been recommended in Ref. [12], one yields $L_{\min} \gg 0.086$ cm. The value of L_{\min} is too small to be used practically. Such a small size of L would bring demerits for the piezoelectric transducer. One can mention the lack of robustness (like electrical, mechanical, and thermal ones) as well as potentially not enough efficiency of light scattering, which is directly conditioned by the size of the transducer. That is why we are forced to consider more appropriate size L , for instance, ten times larger. Consequently, at the frequency $f_3 = 65$ MHz one can use $L \geq 0.86$ cm and expect the Bragg character of AOI.

The acoustic beam diffraction can be considered via estimating the length Z of Fresnel zone for a radiating acoustic aperture R . These values are connected with one another as $Z = R^2 f_3 / (2 V)$ [13]. If it is granted that the acoustic beam belongs to Fresnel acoustic zone and $Z = 6.0$ cm at $f_3 \approx 65$ MHz, one can find that $R \approx (2 V_s Z / f_3)^{1/2} \approx 0.107$ cm for TeO_2 . Thus with $R \geq 0.11$ cm, one can conclude that the expected angular divergence of acoustic beam is definitely small to be neglected. Consequently, the plane-wave approximation can be used for characterizing the acoustic beam propagation. The exact angular divergence of acoustic beam in the tellurium dioxide AOC at $f_3 \approx 65$ MHz can be estimated as well. A reliable spatial size of the initial acoustic beam aperture that we will consider is close to $L \sim 1.0$ cm. Then, one can calculate the angle of acoustic beam divergence $\nu = V / (f_3 L) \approx 9.5 \times 10^{-4}$ rad $\approx 0.0543^\circ$, which is very small.

The TeO_2 -crystal is extremely anisotropic material. Its acoustic anisotropy is illustrated by 2D-surfaces for the phase velocities in the (001)- and $(1\bar{1}0)$ -planes, see Ref. [10, chapter ‘‘Elasticity of crystals’’]. It’s shown there, that the slow-shear acoustic mode has the absolute minimum ($V = 0.616 \times 10^5$ cm/s) with passing along the $[1\bar{1}0]$ -axis. However, the quests for this minimum depend on the chosen plane and exhibit different (by about 3 times from one another) angular behavior. Generally, when an acoustic wave passes through an anisotropic medium, the energy flow can tip out of the wave vector $\vec{K} = K \vec{m}$, where \vec{m} is the unit vector of \vec{K} . Passing the energy flow is characterized by the group velocity vector $\vec{w} = w \vec{s}$, where \vec{s} is the corresponding unit vector, and the group velocity w is equal to the phase velocity V only if $\vec{s} \parallel \vec{m}$. The angle Ψ between the group velocity vector $\vec{w} = V \vec{m} + (I - \vec{m} \vec{m}) \cdot (\partial V / \partial \vec{m})$ and the wave vector \vec{K} is determined by $\cos \Psi = \vec{m} \cdot \vec{s}$. The more the vector \vec{w} tips out of the wave vector \vec{K} , the more the phase velocity V varies with the direction \vec{m} due to $\partial V / \partial \vec{m} \neq 0$, so the angle $\Psi = \arccos(\vec{m} \cdot \vec{s})$ grows from zero. Then, the faster the phase velocity varies with \vec{m} , the farther the vector \vec{w} tips from the vector \vec{K} . Moreover, the vector \vec{w} tips in a direction of growing the velocity, i.e. just outside of a point of a minimal value of the phase velocity in a TeO_2 -crystal [10]. That is why, the presence of small tips of \vec{m} from the $[1\bar{1}0]$ -axis, caused by the acoustic diffraction due to a piezoelectric transducer of finite length L , leads to the above-noted tips of \vec{w} . Thus to find the angular distribution of acoustic energy one has to estimate an additional angular contribution 2Ψ together with the beam divergence ν . A contribution 2Ψ can significantly exceed the contribution of diffraction. At the

same time, the nonlinear character of the phenomenon under analysis within our article makes it very desirable to not add an additional complexity into consideration. To simplify the problem, one has to formulate the requirements to experimental conditions in such a way that the combined effect of acoustic divergence could be excluded from our studies. By this it means that the cross-section of an acoustic beam should be almost the same during its propagation along the optical aperture of a crystal. To avoid not perfectly reliable theoretical estimations for this complicated material we use mainly experimental data in our analysis. On the basis of present knowledge, one can expect the trustworthy estimation from the following experimental data: $2 \Psi_{(a)} \approx 60^\circ$ and $2 \Psi_{(b)} \approx 20^\circ$ in the (001)- and (1 $\bar{1}$ 0)-planes, respectively [2]. Using these approximations, one has to take the cross-section of an acoustic beam with, i.e. $L \approx H \approx 1.2$ cm, i.e. with the cross-section $S = L \times H \approx 1.5$ cm². Such a choice of sizes for the piezoelectric transducer gives $2 \Psi_{(a)} \approx 60^\circ \approx 2.715^\circ$ and $2 \Psi_{(b)} \approx 20^\circ \approx 0.905^\circ$ that promises an acceptable uniformity for the cross-section of an acoustic beam with the tolerance of about 10% along the optical aperture $D \leq 6.0$ cm. (We understand that such an accuracy is not quite well, but it is better than not to carry out further experiments at all due to non-realistic sizes of transducer).

Now, one can estimate potential performances of the tellurium dioxide-made AOC as a dispersive component. The goals are designing similar crystalline AOC and carrying out the needed proof-of-principle experiments with this AOC.

6.2. Acousto-optical figure of merit for the non-collinear three-phonon AOI in the TeO₂-crystal

As it follows from section 4, for the above-chosen geometry in TeO₂ crystal with the declination angle $\vartheta \approx 3.142^\circ$, the ellipticity $\rho \approx 0.37275$, and the slow shear acoustic mode with the acoustic wave vector $\vec{K} \parallel [110]$, one can write $|p_{a \text{ eff}}| \approx 0.655 \times 0.5 |p_{11} - p_{12}| \approx 0.036$, due to $p_{11} \approx 0.074$ and $p_{12} \approx 0.187$ [14]. One may restrict himself by only $p_{a \text{ eff}}$, because only the parameter σ_a has been used in the general solutions, see Eqs.(5) and (6). Because of the material density $\rho_0 \approx 6.0$ g/cm³, $n_O = N_O \approx 2.3297$ and $n_E \approx 2.3301$ at that angle ϑ and $\lambda = 488$ nm, one arrives at the figure of AO merit $M_2 = n_O^3 n_E^3 (p_{a \text{ eff}})^2 / (\rho_0 V^3) \approx 148 \times 10^{-18}$ s³/g. These value of M_2 demonstrates that the anomalous light scattering, governed by the pure slow shear acoustic mode in TeO₂, is sufficiently efficient and this crystal is able to provide effective three-phonon AOI.

Then, the above-chosen first maxima in light distribution require the following optimized power parameters $(\sigma_a x)_{1, \text{opt}, k}$ associated with $f_3 \approx 65$ MHz when $\alpha = 0.1411$ cm⁻¹ and the correction factors of apodization $\kappa_k \approx 1.01139, 1.02443, 1.04345, 1.06867, \text{ and } 1.09884$, respectively. With $x \equiv L$ and $L \approx 1.2$ cm, one can find from Table 1 that $\sigma_{1, \text{opt}, k} \approx 2.588, 2.742, 2.892, 3.033, \text{ and } 3.183$ cm⁻¹. Now, the standard determination for σ [11] with $\cos \theta \approx 1$ can be re-written specifically to the acoustic power density P_1 needed for the first maxima as

$$P_{1,k} \approx \frac{2\lambda^2 \sigma_{1\text{opt},k}^2}{\pi^2 M_2}. \quad (11)$$

Thus, for example at $\lambda = 488$ nm and $f_3 \approx 65$ MHz, Eq.(11) gives the optimized value of $P_{1,k} \approx 20 - 33$ mW/mm², see Table 2.

One can exploit Eq.(10) with $V = 0.616 \cdot 10^5$ cm/s, $L \approx 1.2$ cm, $f_3 \approx 65$ MHz at $\lambda = 488$ nm to estimate the theoretical frequency bandwidths $\Delta f_T \approx 562$ KHz. With this result one can find the theoretically expected spectral bandwidth as $\Delta \lambda_T = \lambda \Delta f_T / f_3 \approx 42.2$ Å as well. Then, using the data related to the frequency and spectral resolution from Table 1, one can obtain the theoretically expected numbers N_k of resolvable spots, see Table 2

Table 2. Theoretical estimations with: $L \approx 1.2$ cm; type of the elastic mode is S [110] with $f_3 \approx 65$ MHz at $\lambda = 488$ nm; the product $\delta\lambda_K = \lambda^2 / (3 b_3 D_K)$ includes the birefringence factor b_3 . Then, $d_{s,k} = \kappa_k \lambda F/D_k$ is an ideal spot size in the approximation of geometric optics

D_k , cm	$\sigma_{1,Opt,k}$, cm^{-1}	B_k , dB	$d_{s,k}$, μm	N_k , res. spots	$P_{1,k}$, W/cm^2
2.0	2.588	2.45	20.976	54.7	2.184
3.0	2.742	3.68	14.164	82.1	2.462
4.0	2.892	4.90	10.821	109.5	2.727
5.0	3.033	6.13	8.866	136.8	3.000
6.0	3.183	7.35	7.596	164.2	3.304

7. RESULTS OBTAINED FROM PROOF-OF-PRINCIPAL EXPERIMENTS WITH THE TeO₂-MADE ACOUSTO-OPTICAL CELL

7.1. Experiment arrangement

First, one can estimate the potential contributions of the acoustic losses for the chosen slow shear elastic mode passing along the [110]-axis, whose displacement vector is oriented along the $[1\bar{1}0]$ -axis. Because of the coefficient of linear attenuation is $\Gamma \approx 290$ dB/(cm GHz²) in a TeO₂ single crystal [9], the factor α [cm⁻¹] of the amplitude acoustic losses is determined as α [cm⁻¹] = 0.1152 Γ [dB/(cm GHz²)] f^2 [GHz]. The carrier frequency $f_3 \approx 65$ MHz at the light wavelengths $\lambda = 488$ nm, specific to the non-collinear three-phonon AOI in tellurium dioxide with the tilt angle $\phi \approx 3.142^\circ$, has been chosen above. Consequently, one can estimate the amplitude factors for linear acoustic losses by γ [dB/cm] = Γf_3^2 , which gives $\gamma = 1.22525$ dB / cm and $\alpha = 0.14115$ cm⁻¹.

Additionally, one has to take into account the losses needed for converting the input electronic signal into an acoustic one, which are usually slightly exceeding 2 dB. However within these our experiments, we have decided to modify the piezoelectric transducer. The practically important problem is connected with relatively narrow frequency and spectral bandwidth of the AOC exploiting the non-collinear three-phonon AOI. The matter is that tellurium dioxide is sufficiently effective AO material, so that the bandshape width of the TeO₂-made AOC can be expanded at the cost of decreasing the efficiency of that AOC. In so doing, the thickness of upper electrode, placed over piezoelectric material, has been a little bit increased to implement the effect of oscillation damping. The goal of such a damping was to decrease the quality factor of acoustic resonance inherent in that piezoelectric transducer. Our experimental estimations have demonstrated that such a damping grew the losses for converting the electronic signal into an acoustic one up to 3.0 – 3.5 dB, while the acoustic resonance curve of that piezoelectric transducer showed a broader maximum.

Previously, we have to restrict ourselves by a maximum level $P \leq 0.5$ W/mm² of acoustic power density. However, novel design of the damped piezoelectric transducer admits the acoustic power density by a magnitude of about $P_1 \leq 3.5$ W/mm² for the acoustic beam cross section of about 1.5 cm² in the AOC under consideration. The produced estimations demonstrate that the above-required levels of the parameters P_1 and $\sigma_{1,Opt}$ for the first unit-level maxima lie in the ranges of accessible values. One can find from Eq.(11) that reaching the next maxima [10] needs much higher acoustic power densities in comparison with the first ones. This looks rather conjectural from the viewpoint of requirements for the electric strength inherent in the available piezoelectric transducer. After that, pre-experimental estimations for the TeO₂-made AOC with $D = 6.2$ cm and $L \approx 1.2$ cm can be summarized in Table 3. These estimations imply exploiting the slow shear elastic mode with the acoustic velocity $V = 0.616 \times 10^5$ cm/s in the scheme of the standard AO spectrum analyzer with the integrating lens of the focal distance $F = 85$ cm.

The design of the tellurium dioxide crystalline AOC under consideration, operating in the regime of the non-collinear three-phonon AOI, is presented in detail in Fig. 12. The piezoelectric transducer represented by a thin plate made of the 163° Y-cut LiNbO₃ single crystal has been placed on the (110) crystallographic plane of the TeO₂-crystal. It provides the excitation of a slow-shear mode acoustic beam with the cross section of about 1.5 cm² and the length $L = 1.2$ cm of interaction in the crystal. The needed Bragg and tilt angles, whose orientations are depicted in Fig. 12, are enumerated in Table 2.

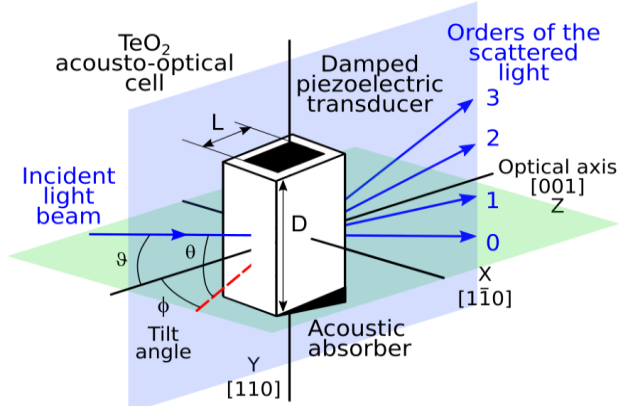


Fig. 12. Design of the tellurium dioxide AOC for the three-phonon AOI.

7.2. Experimental results

Our proof-of-principal experiments has been performed with a wide-aperture Bragg AOC based on the tellurium dioxide single crystal, which has an active optical aperture of about 6.2 cm, see Fig. 13. This pioneer AOC allowed a maximum input acoustic power of about 20 W. It was able to operate over all the visible range starting from the optical wavelength $\lambda = 488$ nm, which combines the convenience of operating in just the visible range with the best-expected performances inherent in this AOC. Practically, we used optical wavelength $\lambda = 488$ nm from the single frequency argon ion laser Innova 300C-I-304 (optical power 0.75 W, Coherent Inc.). The CW-light radiation has the needed elliptic state of the incident light polarization expanded along the crystallographic [110]-axis of the TeO₂-based AOC.

This AOC was prepared to be governed by the radio-wave signals at the central frequency $f_3 \approx 65$ MHz. A set of electronic equipment for both generating and registering the corresponding electric ultra-high-frequency (UHF) radio-wave signals has been exploited. Initially, the UHF-signal, sweeping or tunable as the case requires, was applied to the electronic input port of the AOC through a wide-band UHF-amplifier HD19152 (0.15 – 230 MHz, 20 W) and the corresponding impedance-matching electronic circuits, see Fig. 13.

The optical part of our experiments included a 15-mm Glan-Taylor linear polarizer (the extinction ratio $\sim 10^5$), two rotating polarization plates $\lambda/2$ and $\lambda/4$ (all from Thorlabs), and a four-prism (Edmund Optics) beam expander, which operated as some kind of polarizer as well. This is why first one had to make the required estimations and then to manipulate by both the polarization plates to obtain the elliptic state of the incident light polarization with the pre-assigned ellipticity $\rho \approx 0.3727$. The polarimeter PAX5710 VIS-T (Thorlabs) was used for supervision over light beams. Elliptically polarized light after expander provided rather flat (non-uniformities were better than $\sim 10\%$) initial optical beam profile expanded in the plane of scattering. During the experiments with this beam shaper rather accurate angular adjusting of the incident light beam had been performed. By this it means that both the correct Bragg angle of incidence and the needed tilt angle had been optimized. The 90-mm achromatic doublet lens (Edmund Optics, clear aperture 72 mm, $\Delta\lambda = 400 - 700$ nm) with the focal length of about 85 cm had been used as the integrating lens, and the multi-pixel CCD-linear array (Toshiba) consisting of $4.7 \mu\text{m}$ pixels was playing the role of a photo-detector. The layout of the experimental set-up is presented in Fig. 13, where only the 3-rd order of light scattering pattern is shown.

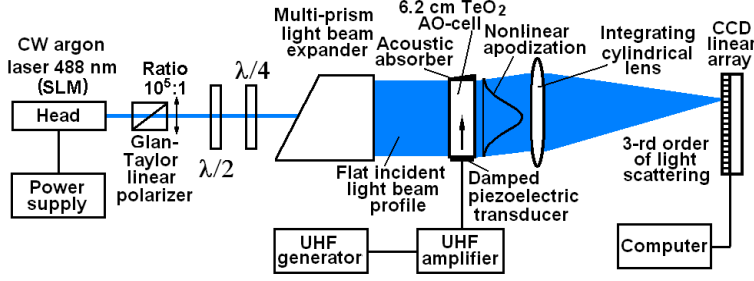


Fig. 13. A layout of the experimental set-up; only the 3-rd order of light scattering is depicted.

The experiments consisted of two parts. The first of them included detecting the frequency bandshape with a low oscillation damping, i.e. determining the effective bandwidth of the Bragg non-collinear three-phonon light scattering at a 0.405-level of light intensity. The second part of those experiments was related to estimating possible spectral resolution within involving this AOC into the optical spectrum analysis. It was done via measurements of individual resolvable spots in the focal plane of the integrating lens for the light deflected by into the third order of scattering. Figure 14 shows an example of the experimental trace for the frequency bandshape inherent in the TeO_2 -based AOC with the damped piezoelectric transducer at the central frequency about 65 MHz, which had been detected under lighting by the light-blue coherent light $\lambda = 488 \text{ nm}$. The total experimental frequency bandwidth at a 0.405-level of light intensity has been estimated by $\Delta f_M \approx 798 \text{ kHz}$. Precise optical measurements have been performed at the wavelength 488 nm to obtain sufficiently reliable estimations for the frequency resolution provided by the TeO_2 -made AOC together with the above-described optical system, including the CCD linear array. The performed measurements have been done with a radio-wave signal applied at the input port of the TeO_2 -cell.

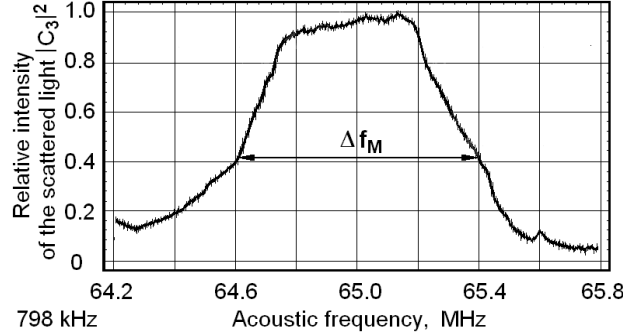


Fig. 14. Experimentally obtained frequency bandshape of the TeO_2 -made AOC at $f_3 \approx 65 \text{ MHz}$ and $\lambda = 488 \text{ nm}$.

As it has been noted, our experimental results have been obtained using the integrating lens with $F = 85 \text{ cm}$ at the wavelength 488 nm, so that theoretically the spot sizes are $d_s^{(4)} = \square \lambda F/D_4 \approx 11.08 \mu\text{m}$ and $d_s^{(6)} = \square \lambda F/D_6 \approx 7.59 \mu\text{m}$. Together with this, the plot in Fig. 15 exhibits the experimental spot sizes $d_M^{(4)} = \square \lambda F/D_M^{(4)} \approx 13.8 \mu\text{m}$ and $d_M^{(6)} = \square \lambda F/D_M^{(6)} \approx 9.45 \mu\text{m}$, respectively, that correspond to the aberration factor $\zeta_M \approx 1.2437$ (which includes various optical demerits of the used wide-aperture crystal and our optical system), and consequently, to the effective apertures $D_M^{(4)} \approx 3.21 \text{ cm}$ and $D_M^{(6)} \approx 4.81 \text{ cm}$ for the AOC [$\kappa_k \approx 1.01139, 1.02443, 1.04345, 1.06867, \text{ and } 1.09884$, respectively, $F = 85 \text{ cm}$, and $D_k = \{2.0, 3.0, 4.0, 5.0, \text{ and } 6.0\} \text{ cm}$].

The TeO_2 -crystal has rather high refractive indices. For example, the main ones are about $n_o = 2.3297$ and $n_E \approx 2.3301$ at $\lambda = 488 \text{ nm}$ used during the experiments. This is why one can expect significant optical attenuation inside the crystal and remarkable reflections from the facets of TeO_2 -

based AOC. Undoubtedly, to minimize potential optical losses the facets of similar AOC ought to have anti-reflection coating [11]. Nevertheless, we have performed our proof-of-principle experiments with the AOC that have not been coated. Therefore, the relative efficiency of light scattering into the third order had been first experimentally estimated and then measured at the output facet of the AOC. In so doing, the light intensity detected at the output facet, transmitted through the cell in the absence of an external UHF electronic excitation, had been counted as the unity. The light intensity scattered into third order in the presence of that electronic signal and measured at the output facet had been considered as the usable optical signal caused by UHF electronic signal. The ratio of this usable optical signal to the initially transmitted light intensity (both are measured at the output facet of that AOC), one can consider as the relative efficiency of AOI. Thus the relative efficiency, determined as it has been described above, had been measured at the optimal acoustic frequency about $f_3 \approx 65$ MHz at $\lambda = 488$ nm. The maximum relative efficiency at the optimal acoustic had been experimentally estimated by the value ~ 0.92 .

Figure 15 depicts two from a set of experimentally obtained light intensity profiles with the spot sizes of about 13.8 and 9.5 microns with the side lobe levels of $\leq 3.5\%$, which include affecting the light distribution in these spot by the acoustic losses of ~ 4.90 and 7.35 dB / aperture, respectively. These profiles had been observed from optical apertures $D_4 \approx 4.0$ cm and $D_6 \approx 6.0$ cm, using the same 6.2 cm sample of tellurium dioxide crystal. The measurements showed that the main lobes of spots gave lighted areas, which were exceeding two pixels of the CCD-row that provided acceptable resolution of a pattern from viewpoint of the sampling theorem.

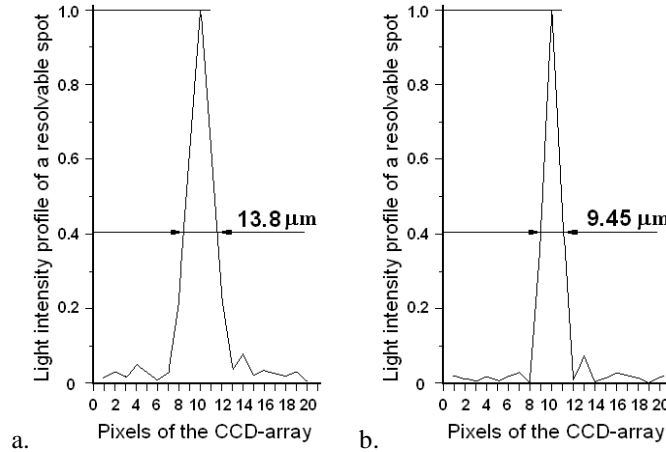


Fig. 15 Light intensity profiles of two individual resolvable spots for the TeO_2 -based AOC at $f_3 \approx 65$ MHz and $\lambda = 488$ nm: (a) $D_{4,M} \approx 4.0$ cm and (b) $D_{6,M} \approx 6.0$ cm.

The last data show that remarkable parts of the active optical apertures inherent in the AOC is lost due to imperfectness of the lens and AOC's crystalline material together with the total effect of linear acoustic losses $B_k = \{2.45, 3.68, 4.90, 6.13, \text{ and } 7.35\}$ dB per aperture. Therefore, instead of theoretical limits of the frequency resolutions $\delta f_{T,k} = V/3D_k$, one yields the measured values $\delta f_{k,M} = V/3D_{k,M}$, which lead to the experimentally obtained magnitudes of the spectral resolution $\delta \lambda_{k,M} = \lambda \delta f_{k,M}/f_3$ at $\lambda = 488$ nm. Then, $\Delta \lambda_M = \Delta f_M \lambda / f_3 \approx 60.05$ Å (instead of the theoretical value $\Delta \lambda_T \approx 42.20$ Å because of damping the piezoelectric transducer). Thus the experimentally obtained numbers of resolvable spots are $N_{k,M} = \Delta f_M / \delta f_{k,M} = \Delta \lambda_M / \delta \lambda_{k,M}$ spots.

In Table 3, the comparison of theoretical and experimental results is presented. One can see that some experimentally obtained data, namely, the frequency and spectral bandwidths as well as the numbers of resolvable spots exhibit general tendency to exceed the above-calculated theoretical values. This tendency takes place despite the presence of natural imperfectness peculiar to all the

optical components in our experimental set-up. Similar results can be attributed to the use of damping the piezoelectric transducer in the developed TeO₂-made AOC.

Finally, the maximal expected lighted length in the focal plane of the integrating lens is $L_{CE} = d_M N_M < 3.0$ mm, i.e. capabilities of the experimental optical system lie in the frames of the exploited multi-pixel CCD-array. Consequently, the best obtained results with the developed TeO₂-made AOC are the spectral resolution $\delta\lambda_M \approx 0.351$ Å at 488 nm and the resolving power exceeding $R_M \approx 13,900$ with the spectral bandwidth $\Delta\lambda_M \approx 60.0$ Å. These data exceed performances of the best acousto-optical spectrometers for space or airborne operations of the twenty-first century [15-17]. However, they does not have a gain compared with our recently obtained results [11] with calomel AOC (the spectral resolution $\delta\lambda_M \approx 0.235$ Å at 405 nm and the resolving power $R_M \approx 17,200$).

Table 3. Comparison of theoretical and experimental data; $\Delta f_T \approx 562$ kHz and $\Delta f_M \approx 798$ kHz; $\Delta\lambda_T \approx 42.20$ Å and $\Delta\lambda_M \approx 60.05$ Å; at $\lambda = 488$ nm

$D_{k,T}$, cm	$D_{k,M}$, cm	κ_k	$\delta f_{k,T}$, kHz	$\delta f_{k,M}$, kHz	$\Delta\lambda_{k,T}$, Å	$\Delta\lambda_{k,M}$, Å	$N_{k,T}$	$N_{k,M}$
2.0	1.59	1.0113	10.27	12.917	0.771	0.970	55	62
3.0	2.35	1.0243	6.85	8.726	0.514	0.655	82	92
4.0	3.084	1.0435	5.13	6.658	0.385	0.512	110	120
5.0	3.76	1.0687	4.11	5.463	0.309	0.411	137	146
6.0	4.40	1.0984	3.42	4.672	0.257	0.351	164	171

Thus our new experimental results for the above-studied TeO₂-made AOC, exploiting the three-phonon AOI, are not better than our recent data [11] obtained within two-phonon AOI in calomel. Although formally the three-phonon AOI has a 1.5-time advantage, in reality the used now and allowing three-phonon AOI TeO₂-crystal exhibits 1.775 times faster acoustic velocity and 1.26 times higher linear acoustical losses, which both have reduced the spectral resolution here.

8. CONCLUSION

The state-of-the-art AO devices based on TeO_2 are applied to various technological needs and very different uses. From precise frequency shifters [18] to optical coherence microscopy using filtering properties of the AO cell [19]. Also, present investigations are focused in improving the characteristics for imaging applications in the mid-infrared range [20], acousto-optical lens [21] and the operation of TeO_2 AO cells in low temperatures for space-borne spectroscopy [22]. All these investigations are related to the Bragg regime for the one-phonon AO interaction. Our present work, in contrast to the avenues of mentioned publications, is towards the use of the three-phonon AO interaction in the Bragg regime.

The three-phonon AOI is the most complicated non-collinear multi-phonon process in an anisotropic crystal. Generally, each direct line, associated with the acoustic phonons, is able to cross a pair of wave-vector surfaces, reflecting two eigen-states of polarization, as a maximum 4 times, indicating 4 orders of light scattering. In the particular case, when these intersections are equidistant, one can observe the three-phonon AOI in Bragg regime. Here, we have developed the most completed up to now theory of this phenomenon and distinguished novel physical aspects specific to its nonlinearity when three-phonon AOI is excited by acoustic waves of finite amplitude. Additionally, we have considered this phenomenon in birefringent crystals exhibiting moderate linear acoustic attenuation. In so doing, specific AO nonlinearity in behavior of the scattered light intensity and frequency mismatch under strongly fixed angular alignment has been identified. These features have been investigated both theoretically and experimentally. Initially, an opportunity of shaping a sequence of the local unit-level maxima under optimal ratio between photo-elastic constants for normal and anomalous processes had been found. Then, a multitude of the transfer function profiles specific to those unit-level maxima in light scattered into the third order have been revealed. We have selected the transfer function inherent in the first unit-level maximum, as a profile that requires the lowest acoustic power to be achieved. Already this profile is able to give us a chance to study the main peculiarities of the non-collinear three-phonon AOI and to analyze preliminarily its applicability for the precise spectrum analysis of optical signals. Such a selection was based on achieving the unit-level maximum in the third order of light distribution that requires a minimal acoustic power for manifesting that nonlinearity. After that, we have found and characterized an additional degree of freedom specific to the non-collinear three-phonon AOI that gives in particular the following. It allows us to achieve close to 100% efficiency with the fixed acoustic frequency for various optical wavelengths due to existing the distinguished birefringence factor inherent in this phenomenon. Moreover, this factor can be varied via choosing the tilt angle whose acceptability depends on the symmetry of a crystal. Owing to the linear interplay between the scattered light and the incident one despite the AO nonlinearity, one can apply the three-phonon AOI to an advanced optical spectrum analysis with the triple accuracy. By this it means that this phenomenon can be taken for developing an advanced approach to the parallel spectrum analysis of optical signals. Therefore, due to three-phonon AOI gives tripling the spectral resolution in the acousto-optics, a possibility for the spectrum analysis of optical signals with the significantly improved resolution has been demonstrated as well.

Under such conditions, only linear acoustic attenuation represents a limiting factor, which restricts potential performances of spectrum analysis. Nevertheless, the effect of moderate acoustic losses has its specific due to its interplay with AO nonlinearity. The analysis have shown that the result of similar interplay leads to appearing the nonlinear apodization. In our case of the fixed acoustic frequency and variable optical aperture, one can obtain various levels of the acoustical losses per the corresponding optical aperture of the AOC to avoid unnecessary strong limitations during the current stage of investigations.

To demonstrate the details of our analysis and to realize possible experiments the crystals of tetragonal symmetry had been considered as examples. Then, very effective (but complicated) AO material, namely, the TeO₂-single crystal had been selected as one of the best options for our goals. The needed theoretical, practical, and pre-experimental estimations have been performed to design a unique wide-aperture AOC based on the TeO₂-crystal. The experiments had been carried out at $\lambda = 488$ nm with various portions of a 6.2 cm-optical aperture AOC based on TeO₂-crystal excited by the slow shear acoustic mode along the [110]-axis. Along with this, we had explored the use of the tilt angle to proceed specific directions for light waves propagation in order to select adequate refractive indices within the AOI. The results of proof-of-principal experiments with this AOC, governed by elastic waves of finite amplitude, confirm in general the previously developed theory and numerical estimations. Moreover, these findings are able evidently to open a new page in the suggested innovative technique for the modern optical spectrum analysis with the significantly progressed spectral resolution based on the three-phonon AOI.

ACKNOWLEDGMENTS

The work was supported by CONACyT, project # 61237 (initially) and Molecular Technology GmbH (Berlin, Germany).

REFERENCES

1. S. Shcherbakov, S. E. Balderas Mata, Je. Maximov, and A. Aguirre Lopez. "The existence of five-wave non-collinear acousto-optical weakly coupled states." *Journal of Optics A: Pure and Applied Optics* 10, pp.1-10, (2008).
2. V. I. Balakshy, V. N. Parygin, and L. I. Chirkov, *Physical Principles of Acousto-Optics*, Radio I Svyaz, Moscow, (1985).
3. V. Yu. Rakovsky, A. S. Shcherbakov, "Multi-phonon Bragg scattering of the light by elastic waves", *Technical Physics* 35 (7), pp. 815-819 (1990).
4. J. Xu and R. Stroud, *Acousto-Optic Devices: Principles, Design and Applications*, (Wiley, 1992).
5. A. S. Shcherbakov, E. Tepichin Rodriguez, A. Aguirre Lopez, "An all-optical 4-bit register based on a four-order scattering of light by coherent acoustic phonons in single crystals", *Mexican Journal of Physics (Revista Mexicana de Fisica)* 50 (3), pp. 297-305, (2004).
6. Korpel. *Acousto-Optics*, 2nd Ed., N.-Y., (Marcel Dekker, 1997).
7. R. W. Damon, W. T. Maloney, D. H. McMahon, "Interaction of light with ultrasound: phenomena and applications," in *Physical Acoustics: Principles and Methods*, W. P. Mason, R. N. Thurston, eds., Vol. VII, pp. 273–366, New York (Academic Press, 1970).
8. N. Uchida, "Optical Properties of Single-Crystal Paratellurite (TeO₂)", *Phys. Rev. B* 4, 3736 (1971).
9. M. P. Shaskolskaya, *Acoustic Crystals*, Moscow, (Nauka, 1982).
10. Yu. I. Sirotnin and M. P. Shaskolskaya, *Fundamentals of Crystal Physics*, (Mir Publishers, 1983).
11. A. S. Shcherbakov and A. O. Arellanes, "Calomel-made crystalline acousto-optical cell designed for an advanced regime of non-collinear two-phonon light scattering", *Opt. Eng.* 55 (3), 037107 (2016).
12. W. R. Klein and B. D. Cook, "Unified approach to ultrasonic light diffraction", *IEEE Trans. Sonics & Ultrasonics*, SU-14, 123 - 134 (1967).
13. A. P. Sukhorukov, *Theory of Waves* (Nauka, Moscow, 1990).
14. C. Chang, *Handbook of Optics*, M. Bass, ed., 2nd ed. (McGraw-Hill, 1994), Vol. II, Chap. 12.
15. V. Y. Molchanov et al., "An acousto-optical imaging spectrophotometer for astrophysical observations," *Astron. Lett.* 28, 713–720 (2002).

16. O. Korablev, J. L. Bertaux, A. Grigoriev et al., "An AOTF-based spectrometer for the studies of Mars atmosphere for Mars Express mission," *Adv. Space Res.* 29, 143–150 (2002).
17. O. Korablev, A. Fedorova, J. L. Bertaux et al., "SPICAV IR acousto-optic spectrometer experiment on Venus Express," *Planet. Space Sci.* 65, 38–57 (2012).
18. A. Dieulangard, J. C. Kastelik, S. Dupont, and J. Gazalet, "Acousto-optic wide band optical low-frequency shifter," *Appl. Opt.* 52, 8134-8141 (2013).
19. S. Machikhin, V. E. Pozhar, A. V. Viskovatykh, and L. I. Burmak, "Acousto-optical tunable filter for combined wideband, spectral, and optical coherence microscopy," *Appl. Opt.* 54, 7508-7513 (2015).
20. S. Valle, J. Ward, C. Pannell, and N. P. Johnson, "Acousto-optic tunable filter for imaging application with high performance in the IR region", *Proc. SPIE 9359, Optical Components and Materials XII*, 93590E (2015).
21. Z. Zhou, L. Li, J. Wang, Q. Hu, and Sh. Zeng, "Beam deformation within an acousto-optic lens," *Opt. Lett.* 40, pp. 2197-2200 (2015).
22. S. N. Mantsevich, O. I. Korablev, Yu. K. Kalinnikov, A. Yu. Ivanov, A. V. Kiselev, "Wide-aperture TeO₂ AOTF at low temperatures: operation and survival", *Ultrasonics* 59, pp. 50-58 (2015).